



OPEN Investigating probe-receptor interactions and enhancing fluorescence guided surgery with fluorescence lifetime imaging and NF-800 in HER-2 positive esophageal adenocarcinoma

Francesca La Cava^{1,3}✉, Francesca Arena^{1,3}, Daniele Faletto¹, Margherita Iaboni¹, Federico Crivellin¹, Alessia Cordaro¹, Miriam Roberto¹, Federica Pozzi¹, Francesco Fersini¹, Giovanni Valbusa¹, Francesco Stummo¹, Mathieu Cinier², Simon Huet², Francesco Blasi¹, Alessandro Maiocchi¹, Luisa Poggi¹ & Erika Reitano¹

FLIM (Fluorescence Lifetime Imaging Microscopy) is a powerful technique used to study protein–protein interactions, enzyme kinetics dynamics, and cellular metabolism. It is also used in studying diseases like cancer, where changes in fluorescence lifetimes can indicate alterations in cellular physiology of malignancies. Recently, FLIM technology in fluorescence guidance has been applied in receptor-targeted clinical applications. Here, we propose the application of FLIM in two animal models of esophageal adenocarcinoma, xenograft and orthotopic with a HER-2 targeting probe (Nanofitin-IRDye800CW, NF-800 hereafter) previously developed. Moreover, the technique was used to further investigate the determinants of lifetime during probe-receptor interactions. The presented data indicates that FLIM is a powerful technique and, when coupled with NF-800, it could enhance tumor contrast, leading to new clinical applications in fluorescence guided surgery.

Keywords Fluorescence Lifetime, HER-2, Nanofitin, Near-Infrared, Optical Imaging

Over the past decade, Fluorescence Guided Surgery (FGS) using targeted-imaging has emerged as an elective method for intraoperative cancer detection and removal. Tumor-targeted FGS made its first clinical trial in 2011¹ and since then, research in this area has drastically increased, creating a new field of studies (including clinical trials) based on the intraoperative visualization of cellular processes to improve cancer surgeries outcomes². Following the success of targeted anticancer drugs, several approaches to FGS tumor targeting have used therapeutic monoclonal antibodies as backbone for probe design^{3,4}. However, their sensitivity remains limited mostly due to their size (more than 150 kDa) and consequently long retention into the bloodstream, resulting in late imaging time points and low tissue contrast, despite the high tumor accumulation^{5,6}. The optimal balance between a rapid clearance and a good image tissue contrast is known to be provided by smaller molecules, such as affibodies⁷, fibronectins⁸, and Nanofitins⁹.

Nanofitins are cysteine-free protein scaffolds derived by the hyper stable DNA-binding protein Sac7d (7 kDa, 66 amino acids) of *Sulfolobus acidocaldarius*. Nanofitins have a high stability to temperature and to a wide range of pH conditions, a fast clearance, and their binding specificity toward a target of interest can be custom-engineered via randomization of the residues initially involved in the binding to DNA. Moreover, Nanofitins are highly tolerant to modification of both their N- or C-terminal ends, including the addition of purification tags or a single cysteine residue, enabling regioselective derivatization of the molecule without affecting its binding properties.

¹Bracco Research Centre, Bracco Imaging SpA, Colletterto Giacosa, Turin, Italy. ²Affilogic Sas, 24 Rue de La Rainiere, Nantes, France. ³Francesca La Cava and Francesca Arena have contributed equally. ✉email: francesca.lacava@bracco.com

HER-2 (Human Epidermal Growth Factor Receptor 2) exhibits characteristics that make it a suitable biomarker for targeted fluorescence imaging in a variety of solid tumors. It is a plasma membrane-bound tyrosine kinase receptor encoded by an oncogene amplified in different types of cancer. In particular, HER-2 is overexpressed in esophageal tumors, with a higher positive percentage in case of adenocarcinoma, with a 17–32% incidence and a higher associated morbidity^{10–12}.

Esophageal cancer is the 8th leading cause of death in the world, accounting to 575,000 cases/year¹³. Prognosis remains poor with 5-year survival in the range of 15–25%, with only small improvements accomplished over the last couple of decades¹⁴. In the first stages, surgical resection is the only treatment available¹⁵. Long term survival of those patients affected with esophageal carcinoma is heavily influenced by lymph node metastasis and the effectiveness of esophagectomy, especially due to the fact that anastomotic leaks increase morbidity. Considering the negative impact of esophagectomy on patient's life quality, there is a strong interest in optimizing the procedure to maximize efficiency. Fluorescence surgical resection could enhance esophagectomy by aiding in primary tumor identification, sentinel lymph node mapping and esophagus perfusion evaluation after anastomosis¹⁶.

Fluorescence Lifetime Imaging microscopy (FLIM) is a technique that exploits a specific property of fluorescence other than mere photon absorption and emission. When a fluorescent molecule is excited by light, it emits light at a longer wavelength (lower energy) than the excitation light. However, the time it takes for the molecule to return to its ground state and stop emitting light is not always instantaneous. This time is called the fluorescence lifetime and is a peculiar property of the fluorescent molecule. The lifetime can be estimated by using several approaches, exploiting the fact that return to the ground state can be fitted with an exponential decay function. This decay rate strongly depends on the molecular environment and changes in molecular conformation. For this reason, FLIM has been used to study cellular and animal metabolism and, often, to generate contrast for fluorescence guided surgery¹⁷.

Unlike fluorescence intensity-based techniques, FLIM is largely unaffected by experimental conditions such as probe concentration and internalization and is often uniquely indicative of the local tissue environment¹⁸. FLIM has been previously applied to enhance tumor contrast with fluorescence probes in different preclinical studies¹⁹ and it has proved to reduce the non-specific fluorescence contributions of tissues, a feature that decreases both sensitivity and specificity of standard fluorescence-guided surgery. Moreover, in 2022, the first clinical trial adopting the FLIM technology was performed with an EGFR probe, Panitumumab-IRDye800, suggesting a strong potential of FLIM for receptor-targeted clinical applications²⁰.

The aim of this work is to investigate probe-receptor interactions using Fluorescence Lifetime Imaging with a small protein-based targeting contrast agent, and to evaluate its potential for improving tumor margins assessment during Fluorescence Guided Surgery. In particular, IRDye800CW was conjugated to an anti-HER-2 Nanofitin. The probe was used to perform FLIM experiments both *in vitro* and *in vivo* on xenografts and orthotopic HER-2 positive models of esophageal adenocarcinoma²¹, using a state-of-the-art in-house lifetime microscope.

Results

In vivo model characterization

In order to investigate whether it was possible to observe a change in lifetime due to the binding of the probe to its receptor *in vivo*, two animal models with increasing complexity (xenograft and orthotopic tumor) were considered.

OE-19 derived tumors were first implanted as xenografts. Animals were treated between 14 and 16 days of implantation, when xenografts reached a mean tumor volume of 400 mm³.

Xenograft tumors of non-treated animals (n = 3) were also cryopreserved and successfully implanted as orthotopic tumors into the esophagus of recipient mice. Tumor growth was monitored via bi-weekly MRI starting 7 days post-surgery. As it is possible to observe from the T_{2w} images of the orthotopic model in Fig. 1, tumor appears to grow along the site of induction, with a tendency to infiltrate into the esophagus and stomach. Macroscopically, when it grows on site, it appears as a globe-like structure clearly defined and identifiable (Fig. 1C). Infiltration seem to properly mimic the clinical development of this type of tumors.

The morphological analysis of excised specimens highlighted the presence of a tumor mass and residual surrounding tissues, esophagus and stomach, confirming that the lesion was developed in correspondence to the induction site. Tumors from OE-19 cells displayed the characteristics of an esophageal adenocarcinoma, in which epithelial tumor cells were organized in a fibrovascular stroma (Fig. S1A). Immunofluorescence staining of an adjacent tissue section showed that HER-2 expression was restricted to epithelial tumor cells with no expression in the surrounding tissues (*i.e.*, tumor stroma, esophagus and stomach) (Fig. S1B).

Tumors were also investigated by Western blot analysis, confirming a good HER-2 expression. Heterogeneity within tumors was to be related to inter-mouse variability (Fig. S2).

In vivo experiments

In vivo selective tumor accumulation of NF-800 was demonstrated upon its intravenous injection in OE-19 xenografts tumor bearing mice (n = 7). NF-800 showed a selective accumulation into the tumor tissue *in vivo* at 4 and 6 h post administration, which was also confirmed by *ex vivo* measurements (Fig. 2A). *Ex vivo* optical images acquired 6 h after administration of NF-800 led to significant accumulation of the probe into the tumor (Fig. 2B). A high fluorescence intensity was also observed in the kidneys as well as in the liver, due to the mechanisms that regulate the excretion of the Nanofitins²².

The lifetime value observed in both kidney and liver was comparable with that of the probe in PBS solution (Fig. 2C), which suggests that the probe is not engaged in a specific interaction with the surrounding tissues. On the contrary, a significant difference (*p* value < 0.0001) was observed between the Fluorescence Lifetime (FLT)

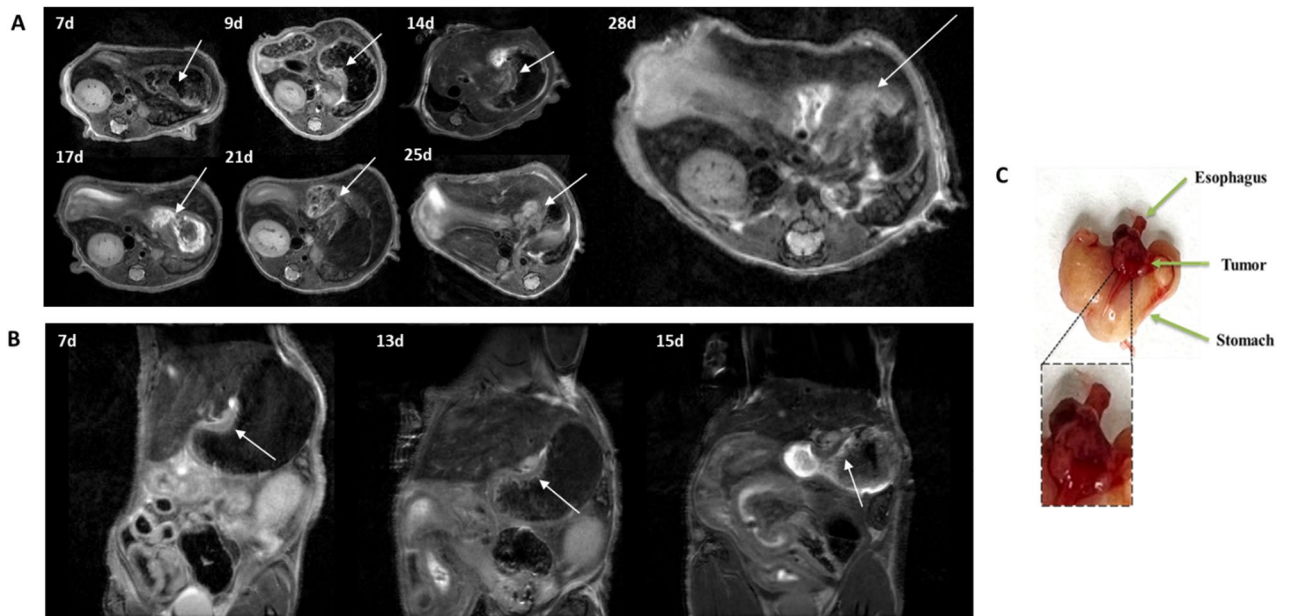


Fig. 1. Representative T_2 -weighted images of (A) animal R02 (axial) and (B) animal R06 (sagittal) showing tumor growth at different time points (arrow indicates the tumor). (C) Representative image of stomach, tumor and esophagus as seen during necropsy.

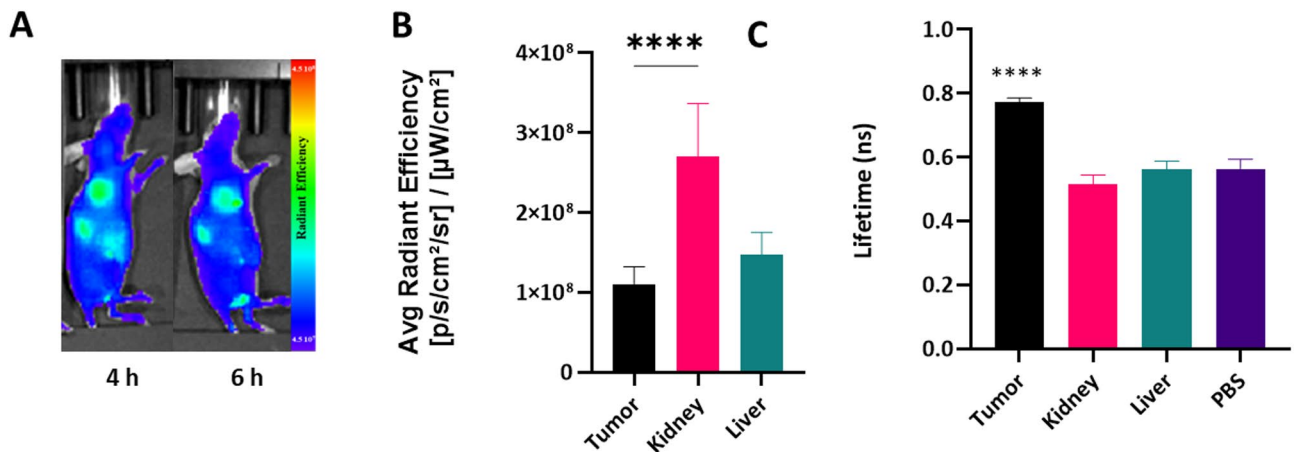


Fig. 2. (A). Representative images of OE-19 xenograft bearing mice imaged at 4 and 6 h post NF-800 injection at IVIS Spectrum. (B) Mean fluorescence intensity values of Tumor, Kidney and Liver of animals bearing OE-19 xenografts and treated with NF-800. (C) Lifetime values obtained with tail fitting of the abovementioned tissues, compared to the probe dissolved in PBS ($n = 7$ animals). One way ANOVA Multiple comparison test ($* = p \leq 0.05$; $** p \leq 0.01$; $*** p \leq 0.001$; $**** p \leq 0.0001$).

value of the excised tumors compared to excised kidneys and livers (Mean tumor Lifetime: 0.77 ± 0.01 ns vs Mean kidney Lifetime: 0.56 ± 0.02 ns and Mean liver Lifetime: 0.51 ± 0.01 ns) (Fig. 2C). The increase in lifetime observed in the tumor could be due to a change in conformation of the probe when bound to the HER-2 receptor and be reflecting the selective engagement of the probe on its target receptor.

In vivo NF-800 specificity towards HER-2 receptors was further confirmed by administration of the probe to mice bearing orthotopic OE-19 tumors. Tz-800 was administered as a positive control, since this probe is known to bind towards HER-2. After 6 h, mice were euthanized, and their organs were collected. In particular, stomach, esophagus, tumor (Fig. S3A) and muscle (not shown) were excised and imaged together at the Explorer Air 1 (EA1) for fluorescence intensity measurements. In Fig. S3A, tumor appears clearly visible in fluorescence images, with a more intense signal than the stomach, despite having a really small size (average dimension of treated tumors was 54.8 ± 19.5 mm³), compared to the surrounding organs. Calculated ex vivo Tumor to background Ratio (TBR) had a mean value of 9.72 ± 3.42 for NF-800, whereas 5.11 ± 1.86 for Tz-800. In this experimental setting, NF-800 performed better than Tz-800 (p value < 0.005) with a TBR almost twice higher (Fig. S3B). This

higher TBR ratio could be attributed to the higher selectivity and greater tissue penetration potential of NF-800 compared to Tz-800, due to the size difference between the two probes. NF-800, with a molecular weight 20 times smaller than Tz-800, has a higher extravasation potential.

Specific binding of NF-800 and Tz-800 to the HER-2 receptor was confirmed by measuring FLT on ex vivo specimens. Since NF-800 tends to have a high renal excretion whereas Tz-800 tends to be eliminated by the hepatobiliary route²³, we chose kidneys and liver for nonspecific binding estimation of NF-800 and Tz-800, respectively. As expected, a significant difference (p value < 0.0001) was observed between the FLT value of the excised tumors treated with NF-800 compared to kidneys (Mean tumor FLT: 0.81 ± 0.06 vs Mean kidney FLT: 0.56 ± 0.02). Similarly, Tz-800 mean lifetime values of tumors and liver were: 0.87 ± 0.02 and 0.73 ± 0.02 ns.

Interestingly, while measured fluorescence intensities in elimination organs (*i.e.*, kidney or liver) are higher than targeted tissues, we could observe a significant difference in the measured lifetimes, demonstrating the benefit of Lifetime fluorescence imaging to discriminate between accumulation in an organ and specific target engagement (Fig. 3). It is worth noting that in the case of the Tz-800, a slight increased lifetime was observed in the elimination organ (liver) with respect to NF-800, likely attributable to possible intrinsic tissue interactions within the structure of the Ab fragments.

FLIM allows direct differentiation between healthy and cancerous tissues. In this matter, parametric lifetime maps can help with visualization of the distribution of lifetime in the observed samples. To achieve this, fluorescence intensity stack images were fitted to determine the lifetime distribution of the pixels. As a result, it is possible to obtain a histogram that shows the distribution frequencies across the whole image, which in turn can be reconstructed as a parametric map (Fig. 4). NF-800 shows a really high specificity, and that can be demonstrated by looking at an example of a representative parametric map of a tumor excised together with its stomach and esophagus of an animal in the experiment. A low FLT value (approx. 0.6 ns) is linked to the stomach, while higher values (approx. 0.7–1 ns) are linked to the tumor, which in this case appears to have spread throughout the organ and is clearly defined and recognizable (Fig. 4). This confirms the specificity of the probe at engaging its HER-2 target in the tumor tissue.

FLIM and WB correlation analysis

Since Fluorescence Lifetime Imaging is indicative of a probe-receptor interaction, we could assume that every pixel in the region of interest corresponding to a lifetime of 0.71 ns could be reporting for the probe bound to the receptor. We correlated HER-2 expression of OE-19 xenograft tumors with the number of pixels that showed a lifetime between 0.71 and 0.72 ns in parametric maps of the same tumors treated with NF-800 ($n = 5$). The examination of potential relationships between FLIM response and HER-2 target concentration, as determined by Western Blot analysis, unveiled a robust positive correlation. The maximum FLIM signal observed between 0.71 and 0.72 ns displayed a Pearson correlation coefficient (r) of 0.75 with the concentration of HER-2 in tumor samples. This substantial correlation indicates a strong linear association between the FLIM response and the targeted protein concentration (Fig. S4).

Fluorescence lifetime in vitro measurements

The molecular determinants of fluorescence lifetime remain incompletely understood. Numerous studies have been conducted, and various hypotheses have been proposed²⁴.

To assess probe ability to change their lifetime as a function of different determinants, we measured solutions of both probes, NF-800 and Tz-800, and their unconjugated dye in different environments: PBS, Human Serum and in presence of 0.66 mg/mL of Bovine Serum Albumin (BSA) (Table 1).

While no systematic study has examined the environmental effects on IRDye800CW, it is well established that the dye can bind to albumin²⁵ and subsequently change its lifetime when it changes in molecular weight.

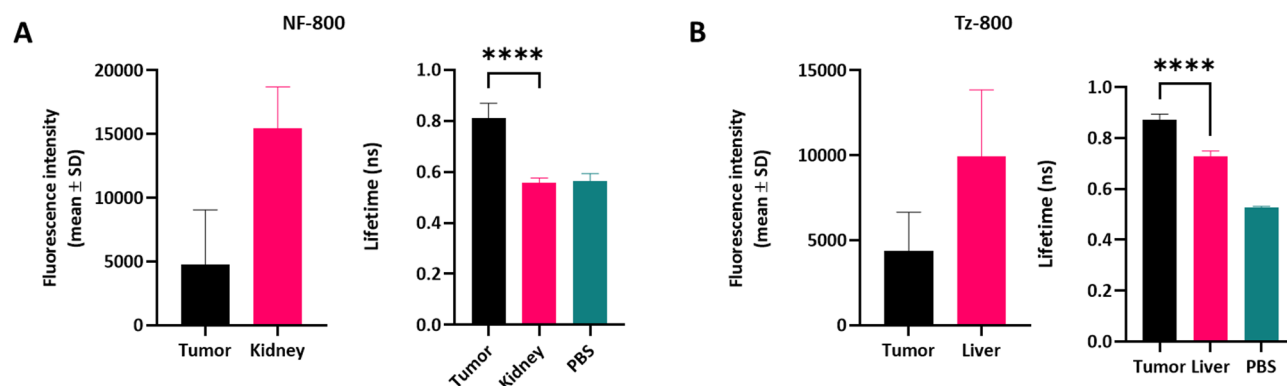


Fig. 3. (A) Fluorescence intensity values (counts) and respective lifetimes (ns) of ex vivo tumor and kidneys 6 h after administration of NF-800. (B) Fluorescence intensity values and respective lifetimes (ns) of ex vivo tumor and liver after administration of Tz-800. (One way ANOVA Multiple comparison test was performed between all the groups (e.g. tumor vs kidney; tumor vs PBS; kidney vs PBS) (* = $p \leq 0.05$; ** $p \leq 0.01$; *** $p \leq 0.001$; **** $p \leq 0.0001$).

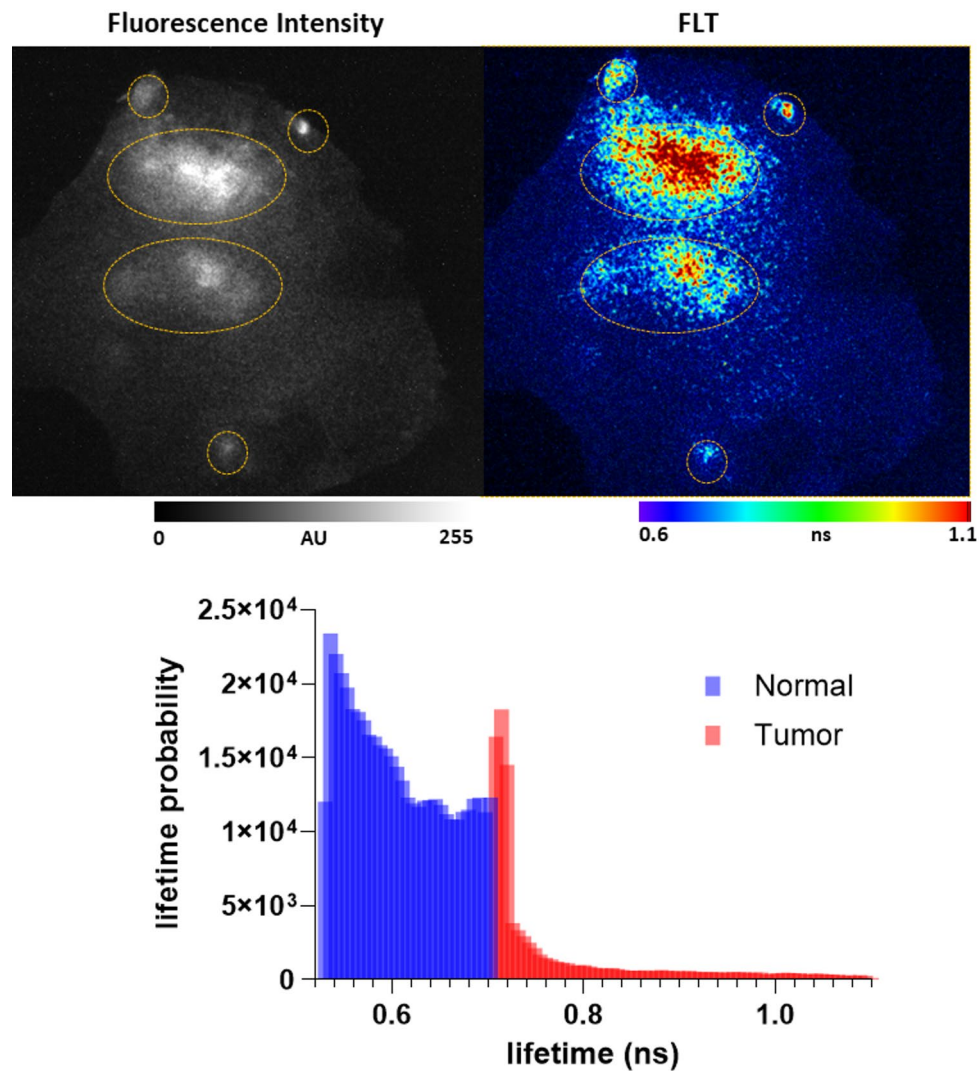


Fig. 4. Representative Fluorescence Intensity (AU) and FLT parametric map (ns) of a tumor treated with NF-800. ROIs indicate tumors, which appears to have spread throughout the stomach. Histogram represents distribution of lifetimes across pixels, as fitted to obtain the parametric map.

Dyes	PBS	BSA	Serum
NF-800	0.44 ± 0.03	0.59 ± 0.01	0.85 ± 0.02
Tz-800	0.53 ± 0.01	0.57 ± 0.01	0.81 ± 0.06
IRDye800CW	0.48 ± 0.04	0.75 ± 0.01	0.83 ± 0.08

Table 1. Lifetime (ns) mean values and standard deviation of the fluorophore IRDye800CW, unconjugated or conjugated to a targeting moiety, in PBS, BSA and Serum.

As expected, a doubling in lifetime values (0.48 ± 0.04 ns vs 0.75 ± 0.01 ns) was observed when IRDye800CW was in presence of albumin: binding of the dye results in a change of molecular size, which in turn leads to an increased residence time in the excited state.

Remarkably, lifetime values for both probes, NF-800 and Tz-800, in the presence of BSA did not change: conjugation of the dye to the binding moiety impaired in some way the ability of the fluorophore to bind albumin or, our probes could bind bovine albumin but display multi-exponential decays, probably due to the presence of several binding regions²⁶. Conversely, the lifetimes of NF-800 and Tz-800 were approximately twice as long in human serum compared to PBS, suggesting that both probes are affected by the viscosity and protein content of the serum, which could in turn have an effect on their associated fluorescence decay.

Just as what is assumed for the binding to albumin, targeting probes are expected to display multiexponential decays in the case of the specific and strong interaction with their receptor. Near Infra Red (NIR) polymethine

Solvent Orientation Polarizability

Fluorophores	Solvent Orientation Polarizability					
	0.32 PBS	0.31 Met-OH	0.29 Et-OH	0.28 Acetone	0.26 DMSO	0.14 Chloroform
ICG	0.26±0.01	0.37±0.01	0.54±0.01	0.58±0.01	0.82±0.03	1.05±0.01
IRDye800CW	0.46±0.02	0.80±0.04	0.88±0.01	1.05±0.02	1.13±0.03	*
Tz-800	0.58±0.01	0.63±0.01	0.69±0.01	0.49±0.02	1.13±0.04	0.88±0.01
NF-800	0.53±0.01	0.73±0.04	0.79±0.01	*	1.12±0.03	0.62±0.06

Hydrophilic pocket Hydrophobic pocket

Table 2. Lifetime of ICG, IRDye800CW, NF-800 and Tz-800 vs solvent orientation polarizability. Yellow columns indicate the polarizability of the hydrophilic pocket, green columns indicate the hydrophobic pocket. The asterisk (*) indicates missing values due to fluorophore quenching.

Dyes	Glycerol content			
	100%	50%	25%	0%
ICG	0.63	0.41	0.32	0.26
IRDye800CW	0.90	0.52	0.50	0.48
Tz-800	0.73	0.76	0.74	0.53
NF-800	0.69	0.64	0.66	0.44

Table 3. Observed lifetime (ns) values of fluorophores dissolved in increasing glycerol content.

dyes are known to be able to exhibit either a short (0.4–0.7 ns) or long (0.9–1.3 ns) lifetime component binding albumin via two binding sites with different sizes and polarities²⁷. This may be due to the fact that the binding site, or, in other words, the binding site microenvironment could have a difference in polarity, polarizability or dielectric constant, which directly affect the lifetime of the fluorophore. We could imagine that, if a fluorophore were to bind to a hydrophilic pocket, it would display a lifetime which could be different compared to when bound in a more hydrophobic environment.

In order to see if it was possible to understand the nature of HER-2 binding site of NF-800 and Tz-800, both probes, together with IRDye800CW, were dissolved in different solutions with increasing polarity (Table 2). ICG was used as a control, since the experiment was performed as already published by Berezin *et al.*²⁷. As expected, there was a curvilinear increase in lifetime as solvent polarity decreased.

The approximate polarity of binding sites is quite known²⁸: a hydrophilic pocket has an orientation polarizability between 0.28 and 0.30, while a hydrophobic pocket should be between 0.16 and 0.20. By taking into account the lifetime measured in a reference polarity, as reported in Table 2, we can assume that if our probe were to bound to that pocket, the lifetime of the probe interacting with the receptor should be comparable to the one measured in a reference polarity. NF-800, that seems to bind to a different HER-2 pocket than Trastuzumab²⁹, had a bound lifetime which was superimposable to the one in EtOH. Trastuzumab binds HER-2 to its IV extracellular domain, which is hydrophobic³⁰. For this reason, we could expect bound Tz-800 to have a lifetime comparable to lower solvent polarities. The observed lifetimes of Tz-800 follow the same trend of IRDye800CW and NF-800. However, there are significant differences between Tz-800 and the other two fluorescence molecules. Hence, we can assume that Tz-800 change in lifetime could be more influenced by restriction of movement (another known determinant of lifetime) than polarization, meaning that the fluorophore contribution to the lifetime could depend more by interaction than polarity of the environment.

The influence of the restriction of movement of the probes was demonstrated by increasing environmental viscosity (Table 3). Probes and dyes were dissolved in solutions with increasing glycerol content. Lifetime was measured shortly after.

It has already been demonstrated that viscous surrounding is expected to restrict vibrational and rotational freedom of the molecule, in both excited and ground state, leading to partial elimination of the non-radiative pathways. This results in an increased lifetime due to a higher fluorescence efficiency.

As expected, all molecules vary their lifetime as a function of the environmental viscosity. However, this happens to various degrees. Since probes (Tz-800 and NF-800) have a higher molecular weight, they are affected by small amounts of glycerol, whereas their dye, IRDye800CW, has a restricted vibrational and rotational movement only in high viscosity environments (100% of glycerol content). However, lifetime of NF-800, when bound to its receptor, is slightly higher than what we observed in a complete viscous environment (0.81 vs 0.69 ns): it can be concluded that NF-800 is influenced by both restriction of movement and polarity of the binding site. Tz-800 on the contrary, is influenced primarily by viscous surroundings. Moreover, we can postulate that NF-800 binds to a specific hydrophilic site of the receptor, while Tz-800, as reported in the literature, shows

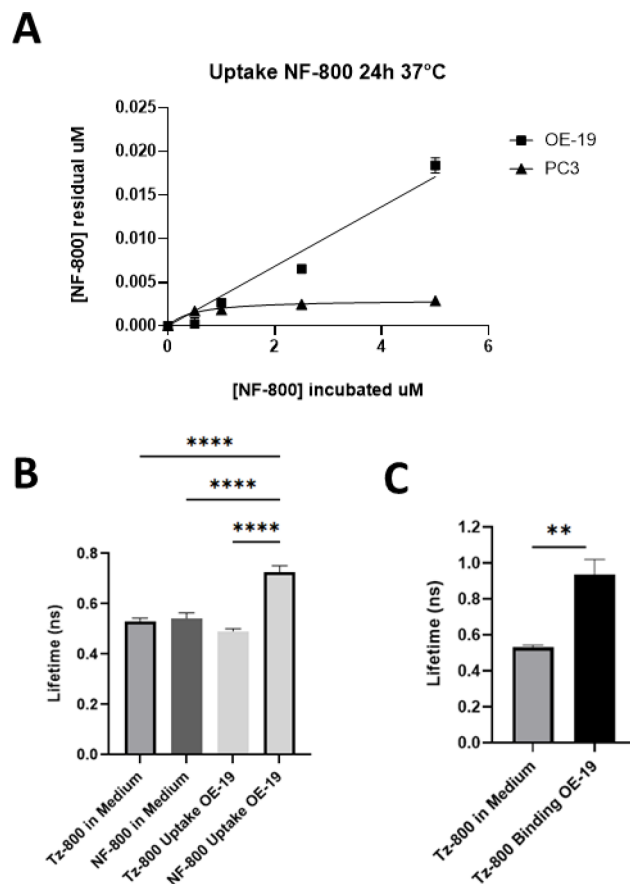


Fig. 5. (A) NF-800 incubated in serum-free medium with OE-19 and PC-3 cells in suspension for 24 h at 37°C at the concentration of 0.5–1.0–2.5–5 μM . (B) Lifetime measurements of uptake experiments performed in OE-19 cells where NF-800 and Tz-800 were incubated. (C) Binding experiments results of Tz-800. One way ANOVA Multiple comparison test (* = $p \leq 0.05$; ** $p \leq 0.01$; *** $p \leq 0.001$; **** $p \leq 0.0001$).

a lifetime in line with the hydrophobicity of its well known HER-2 binding domain. Of note, it was already reported that NF-800 and Tz-800 do not share the same receptor binding site³¹.

In vitro cell measurements

Tumor cell specificity of the FLIM technique and the consequential binding of NF-800 was tested by in vitro measurements using the OE-19 esophageal adenocarcinoma cell line, widely known to overexpress HER-2²⁷. Tz-800 was used as a positive control.

NF-800, Tz-800 and IRDye800CW were incubated at different concentrations (of 0.5–1.0–2.5–5 μM) in a suspension of 8×10^5 OE-19 or PC-3 cells at 37 °C for 24 h. Figure 5 showed the results obtained from the fluorescence acquisitions performed at IVIS Spectrum. Fluorescence intensity signals were interpolated with a calibration curve that allowed to measure the residual concentration of the probes after 24 h (Fig. S5). NF-800 tends to have a higher efficiency compared to Tz-800 (maximum residual concentration: 0.0184 μM for NF-800, Fig. 5; 0.0156 μM for Tz-800, Fig. S6). From that it was possible to calculate the maximum concentration of probe internalized, which was around 3 pmol for Tz-800, and 3.68 pmol for NF-800. As expected, fluorescence intensity signals obtained by PC-3 non-expressing HER-2 cells were negligible, since those cells are known to not to express the target³².

The fluorescence signal associated with cells treated with the unconjugated IRDye800CW was way below the Limit of Detection (LOD) of the instrument, thus it was not possible to measure the fluorescence lifetime FLT of the dye. For this reason, the FLT of the dye dissolved in PBS was used as reference.

Uptake was visible for both NF-800 and Tz-800, while IRDye800CW confirmed the absence of specificity towards the target. Results obtained for NF-800 were further confirmed as shown in Fig. 5B–C, where fluorescence lifetime values are reported. Cells treated with NF-800 showed a higher uptake, which resulted in longer lifetime values (0.71 ± 0.01 ns). Unexpectedly, this was not true for Tz-800: lifetime values after a 24 h uptake were comparable to that of the unconjugated dye in PBS (0.49 ± 0.01 ns) (Fig. 5B). However, this may be due to the fact that the fluorescence decay is known to be highly influenced by viscosity³³, and the cell microenvironment could influence Tz-800 lifetime once internalized (as already observed in the abovementioned experiment, where lifetime in acetone, which is low on viscosity, is compatible to the lifetime of the probe in a non-interacting environment).

Tz-800 interaction with the HER-2 receptor was demonstrated with an experiment of cell binding, where Tz-800 was incubated in suspension with OE-19 at 4°C for 4 h. In this experiment, calculated mean FLT values were 0.94 ± 0.08 ns, confirming a presence of interaction of Tz-800 and the HER-2 receptor, as observed with fluorescence intensity experiments (Fig. 5C).

Since NF-800 lifetime in cells was similar to what was reported in literature for probes conjugated with IRDye800CW²⁰, *in vitro* experiments may indicate a HER-2 specific uptake of the probe.

Discussion

Time resolved fluorescence imaging provides a unique contrast mechanism to monitor key biological processes and enhance tumor-targeting applications. With its higher sensitivity to chemical structures of probes and their surroundings, FLIM analysis of exogenous NIR probes provides information about the tumor microenvironment. Moreover, by eliminating the background signal, which can be readily identified, FLIM adds more information regarding probes distribution compared to conventional fluorescence imaging, which cannot distinguish between tumor specific fluorescence and nonspecific accumulation in the healthy tissue.

As already published in our previous work²⁷, we successfully designed a new fluorescence probe targeting HER-2, constituted of an engineered protein of 7 kDa, Nanofitin³⁴, conjugated to the fluorophore IRDye800CW, namely NF-800. The probe showed a strong *ex vivo* signal even in a small tumor such as an orthotopic esophageal adenocarcinoma into mice, highlighting its potential for conventional fluorescence guided surgery applications.

We then demonstrated the feasibility of using fluorescence lifetime imaging in fields that are gaining new traction, such as Fluorescence Guided Surgery, where FLIM was applied to ICG labeled tumors to improve the accuracy of cancer surgeries³⁵. We demonstrated that FLIM could be useful even during *in vitro* experiments, to better understand the chemistry behind probe – receptor interactions, and *in cellulo*, to better characterize probe uptake and internalization.

Furthermore, we investigated the mechanisms that underly the change of lifetime when a probe is bound to a receptor. As already mentioned by Pal et al., the lifetime change observed *in vivo* could be due to a higher lysosomal viscosity because of a subsequent internalization into cells after binding to the receptor of interest. Our experiments demonstrated that lifetime technique could give itself a lot of information regarding what happens to a fluorescent probe during its interaction with the receptor, even on an *in vitro* level. For example, it was possible to confirm the nature of the pocket in which both NF-800 and Tz-800 bind: by taking into account the reference binding lifetime observed both *in vivo* and *in cellulo*, we can identify the polarity of the binding site, which is hydrophobic for Tz-800, and hydrophilic for NF-800. Moreover, by dissolving the probe of interest in increasing glycerol content, it was possible to further assess the nature of the intracellular microenvironment once a probe interacted with the receptor. Both NF-800 and Tz-800 change their lifetime with increasing glycerol content. However, NF-800 lifetime in glycerol at 25% is slightly lower than the bound lifetime in tumors (mean value of 0.66 ns vs 0.81 ns), suggesting that NF-800 lifetime is influenced by more than one environmental factor. Tz-800 instead, has a value in glycerol 25% which is closer to the lifetime value in tumors (mean value 0.74 ns vs 0.87 ns), suggesting a more prominent dependence on viscosity than polarity. If confirmed with further experiments, Tz-800 could be used as a lysosome-viscosity sensitive fluorescent probe³⁶. Other lifetimes determinants, such as quenching, pH and temperature were not investigated into the work, but may further confirm what was observed.

FLIM could enhance tumor contrast by reducing the background signal and highlighting the probe specificity. Thanks to our in-house-built microscope, it was possible to distinguish between healthy and tumor tissue, even in tumors as small as 15 mm³ in size. Moreover, since FLIM measurements are not completely affected by tissue light propagation, we could attribute the change in lifetime only to the probe bound to the tumor, thus eliminating any unspecific signal coming from the background by using IRF and subtracting the background (which corresponds to the signal of noise or scattered light) in image fitting, even in deep tissues or in cases of tumor dissemination. This was further demonstrated by correlating the lifetime distribution of NF-800 treated xenograft tumors with the quantification of HER-2 expression by Western Blot: even if it is not possible to identify the single molecule of NF-800 binding to the receptor, it is possible to demonstrate that there is a direct correlation between HER-2 expression and mean lifetime, when comparing an *in vivo* region of interest and a WB analysis on the whole tumor. Specific uptake is clearly visible from just a lifetime parametric map and correlates with HER-2 expression in tumors. A limitation of this study was however the missing correlation of fluorescence intensity and lifetime on histology slices due to a low resolution of our microscope, which is built for *in vivo* acquisitions.

It has already demonstrated that FLIM could be used to assess tumor margins with the help of machine learning, for example, via the use of Computer-aided Diagnosis (CAD) algorithms, that could extrapolate in real time lifetime values from the surgical bed^{37–39}, and the use of this technique has been applied to the clinic with an EGFR antibody coupled with IRDye800CW²⁰.

Our data suggests that time resolved imaging using exogenous contrast agents could improve the resection of tumors on the surgical bed. However, the technique has some limitations. Currently, commercially available clinical microscopes are not equipped for this kind of analysis. Lifetime microscopes are highly expensive, and the camera resolution required for an accurate analysis is usually very high. Nonetheless, this study demonstrated that, with an efficient probe, accurate information can be obtained even with a camera of a resolution as low as 11.72 μm. Moreover, we achieved comparable results *in vitro*, despite the typically lower signal intensity compared to *in vivo* experiments.

Another limitation of the technique is the difficulty of designing new dyes in the NIR window which are able to change their lifetime upon interaction with a large protein, such as a receptor. To this day, no research has been published on this topic. However, IRDye800CW is a user-friendly and commercially available fluorophore that can be conjugated to use in different targets. Specificity of such targeting probes toward the tumour

microenvironment might directly grant selective changes in lifetime that would allow for tumour delineation *in vivo*.

In summary, we showed that it is possible to investigate probe-receptor interactions using Fluorescence Lifetime Imaging with a small protein-based targeting contrast agent, NF-800, and to evaluate its potential for improving tumor margins assessment during Fluorescence Guided Surgery. The probe was used to perform FLIM experiments both *in vitro*, to further investigate the nature of the intracellular environment and *in vivo*, on HER-2 positive models of esophageal adenocarcinoma.

Overall, the results reported here may have important implications for HER-2 overexpressing tumors, especially those with high morbidity, such as those from the gastrointestinal junction, which are usually difficult to remove and to diagnose.

In the future, FLIM technology—especially when coupled with Artificial Intelligence^{40,41}—could pave the way for new applications in fluorescence guided surgery, facilitating more precise tumor margins resection.

Methods

Probes characterization

Sample preparation: IRDye800CW, NF-800, Trastuzumab-IRDye800CW (Tz-800) and ICG (VerDye, Diagnostic Green GmbH, Germany) were dissolved in PBS, DMSO, BSA, Human Serum (Seronom, Sero AS), Methanol, Ethanol, Acetone or Chloroform to a final concentration of 1 μM . Lifetime reading was performed at room temperature by using flat black 96-well plates (Tecan).

Nanofitin conjugation to IRDye800CW-maleimide

Anti-HER-2 Nanofitin shows a single cysteine at its C-terminus. Reduction of the cysteine occurs in the presence of TCEP (9.8 mM TCEP + PBS as reaction buffer) for 1 h at room temperature. Then, IRDye800CW-maleimide (Li-Cor) was added in excess (molar ratio dye-maleimide:nanofitin 3:1), and the reaction was allowed to proceed for 5 h. The conjugation mix was applied into a SEC column (Sephacryl S100 HR, 16 \times 600 mm, Cytiva) previously equilibrated with PBS. The fractions containing purified Nanofitins NF-800 were pooled together and filtered in sterile conditions on a 0.22 μm membrane. Final concentration was determined by UV-Vis (Lambert-Beer Law) using the molar absorption coefficient of IRDye800CW, $\epsilon = 240,000 \text{ M}^{-1} \text{ cm}^{-1}$ (at 780 nm).

Cell culture

Human esophageal adenocarcinoma cell line (OE-19) was supplied by DMSZ (German Collection of Microorganisms and Cell Cultures GmbH, Leibniz Institute). Mycoplasma-free tested cells were grown in RPMI medium supplemented with 10% fetal bovine serum, 2 mM glutamine, 100 IU/mL penicillin and 100 $\mu\text{g}/\text{mL}$ streptomycin. Human prostate adenocarcinoma cell line (PC-3) was supplied by ATCC. Cells were grown in Hams F-12 medium supplemented with 10% fetal bovine serum, 2 mM glutamine, 100 IU/mL penicillin and 100 $\mu\text{g}/\text{mL}$ streptomycin.

Lifetime acquisitions

Lifetime Fluorescence Images were acquired with an in-house built Time Gated Widefield Fluorescence Microscope. The source is a Super Continuum pulsed laser (from NKT Photon), emitting in the wavelength range of 450–1200 nm. An optical fiber connects the laser with the body of the stereo zoom microscope (AxioZoom from Zeiss). The excitation and emission light were selected by equipping the microscope with an IRDye800 filter cube (excitation filter FF01-747/33, dichroic mirror FF776-Di01, and emission filter FF01-776/LP). The repetition rate of the laser is tunable (set at 150 kHz) and probed the external trigger to the delay generator (DG645 from SRS). The delay generator output was used to trigger and synchronize the gated Image Intensifier units (ICCD C9546 from Hamamatsu—working frequency was 30 kHz) and the Digital CMOS camera (C11440-36U from Hamamatsu). The gating window was set to 5 ns with a time step of 0.25 ns applied between consecutive time points. The entire FLIM image sequence covered a time window of about 10–25 ns around the fluorescence peak. Gain and exposure were adjusted accordingly to peak fluorescence intensity to obtain an adequate signal.

In vitro cell experiments

Uptake Experiments were performed by incubating in serum-free medium 8×10^5 OE-19 cells in suspension, up to a final volume of 400 μL . NF-800, Tz-800 and IRDye800CW were incubated for 24 h at 37°C at the following concentrations: 0.25 – 0.5 – 0.75 – 1.25 – 1.5 – 2 μM . After the incubation time ended, cells were washed three times with PBS and then transferred in flat black 96 multi-well plates.

Binding experiment was performed as previously stated, but only for Tz-800 and IRDye800CW, at 4°C and the following concentrations were used: 0.5 – 1 – 2.5–5 μM .

Animal models

Procedures were performed according to the national and international laws on animal research (L.D. 26/2014; Directive 2010/63 EU) and in accordance with ARRIVE guidelines. Projects were approved by Italian Ministerial authorizations under the following projects: 478/2021-PR (xenograft model), 227/2022-PR and 543/2022-PR (orthotopic model). Athymic female nude mice were obtained from Envigo RMS.

OE-19 xenograft model: 5×10^6 cells were resuspended in 0.1 mL of serum-free medium and injected subcutaneously in the right flank of 9 weeks old female Athymic nude mice ($n = 10$), in general gas anesthesia (SevoFlo, sevoflurane). Tumor development was followed by caliper measurement twice a week, from 7 days after induction. Tumor volume was calculated according to the formula: $(L \times W^2)/2$, where L and W are the maximum length and width of the tumor. 3 animals were used as donors of the fragments for the preparation

of the orthotopic model by surgical implantation and for HER-2 determination via Western Blot. Tumors were explanted after sacrifice of the animal using aseptic technique. Fragments of $\sim 4\text{mm}^3$ were cryopreserved in liquid nitrogen using a mixture of 10% DMSO and 90% FBS and stored until future use.

Orthotopic esophageal adenocarcinoma: naive mice ($n = 20$) were orally administered with Mouse MD Placebo Tablets for two days before surgery (1 tablet/mouse/day). The night before surgery, placebo was substituted with Baytril 0.5 mg Tablets and kept up to 4 days after surgery. The surgical procedure was conducted under systemic anesthesia (Rompun 5 mg/kg and Zoletil 50/50 40 mg/kg). OE-19 derived cryopreserved tumor fragments were thawed in RPMI free medium and kept at 37°C up to 60 min until surgical implantation. Exposure of the esophagus was performed via transversal incision of 1 cm of the abdominal epigastric region. Stomach and liver were gently moved with the use of DeBakey atraumatic forceps to expose the abdominal esophagus; particular attention was given to the vagus nerve, which runs parallel to the esophagus and may cause Dilated Gastric Emptying or oropharyngeal dysphagia if damaged. The esophageal serosa was gently damaged with forceps and one tumor fragment (approx. 4mm^3) was sutured using an 8.0 prolene suture; Buprenorphine was administered subcutaneously (0.05 mg/kg) the late afternoon of the surgery and in the two successive days; Carprofen (5 mg/kg) was administered 24 h after the surgery and in the two successive days. Animals were sacrificed by overdose of sevoflurane anesthesia, confirmed by cervical dislocation, at the end of the experimental phase.

MRI experiments

MRI T_{2w} images were acquired with a Pharmascan 7 Tesla scanner (Bruker Italia) equipped with a quadrature volume rat head coil. During all MRI experiments, animals were anaesthetized with sevoflurane gas (about 1%) in O_2 . Anesthesia was maintained by adjustment of gas level in function of breath rate. The MRI acquisition protocol for tumor development was carried out at 7 T and it required the acquisition of T_2 weighted sequences at least twice a week, from 7 days after tumor implant. Regions of Interests (ROI) were drawn on the tumor of T_{2w} sequences to measure the volume (mm^3).

Optical Imaging experiments

Animals were fed with VRF1 (P) sterile diet. Then at least five days before treatments, AIN-76a rodent diet irradiated, a special diet that reduces auto-fluorescence, was used up to the end of the experiments. For animals bearing an orthotopic tumor, the same diet was added also in liquid form.

Mice bearing xenografts with at least 300mm^3 of tumor volume ($n = 7$) were administered with NF-800 at a dose of 10 nmol/mouse in an administration volume of 0.1 mL at an injection rate of about 1 mL/min. Mice were sacrificed after 6 h of administration of fluorescent probes. Fluorescence intensity acquisitions were performed at IVIS Spectrum (Perkin Elmer Italia S.p.A.) equipped with an excitation filter at 745 nm and emission filter at 800 nm with 30 nm and 20 nm bandwidth, respectively.

Mice bearing orthotopic tumors of at least 30mm^3 were administered with NF-800 at a dose of 10 nmol/mouse ($n = 10$) and Tz-800 at a dose of 0.5 nmol/mouse ($n = 5$) in an administration volume of 0.1 mL at an injection rate of about 1 mL/min. Mice were sacrificed after 6 h of administration of fluorescent probes. Fluorescence intensity acquisitions were performed at Explorer Air 1 (SurgVision GmbH, Germany) on tumor, stomach, esophagus and muscle with an excitation filter at 760 nm and emission filter at 819 nm ($\pm 22\text{nm}$ bandwidth).

Image analysis

Regions of interest (ROIs) were drawn on the tumor image and on a reference background healthy region (hind limb muscle) of the mouse for each fluorescence image at every time point to evaluate signal intensity in the tissues. The ratio between the fluorescence signal in the tumor and background healthy tissue (TBR) was then calculated to assess the contrast.

Image stacks of in vitro experiments and ex vivo tissues obtained from time-gated Lifetime Fluorescence Images were analyzed using a software developed in-house in Python. ROIs were defined manually, and average pixel intensity was calculated. Fluorescence Lifetime (expressed in ns) was measured using a tail fitting method that ignores Instrument Response Function (IRF) and takes into consideration only the tail of the decay curve. Subtraction of background signal was performed by manually selecting the ROI where signal was present. Truncation was performed acquiring the first experimental image and selecting the specific starting point for the tail fitting analysis with a GUI slider. The identified point was then used for all subsequent analyses to ensure consistency throughout the study.

Lifetime parametric maps of ex vivo images were obtained by using FLIMFit 5.1.1, a MATLAB (MathWorks, Natick, Massachusetts, United States)-based software tool, developed at Imperial College London, UK (<https://flimfit.readthedocs.io>). Fitting of the images was performed by using a Pixel-wise Global fitting method based on a Maximum Likely Estimate algorithm; IRDye800 IRF was used as a reference to fit the data. IRFs and images were pre-processed by transforming the stacks in time-function hyper stacks with ImageJ software, that were then converted in OME-TIFF format. Metadata were changed by using command window Bio-Formats tools 8.3.0 (Glencoe Software Inc.; <https://www.openmicroscopy.org/bio-formats>). Background subtraction was performed by selecting on the interface the value of 200 counts, which corresponds to the noise in the acquired images. Goodness of fit was estimated by calculating reduced chi square.

Histology

Excised OE-19 orthotopic tumors, together with residual surrounding tissues were embedded in OCT (Optimum Cutting Temperature) resin and frozen in isopentane cooled down in liquid nitrogen. Tumors were then sectioned at $10\text{ }\mu\text{m}$ -thick slices using a cryostat (Leica Biosystem) at different levels. One slide for each tumor level was processed with standard Hematoxylin and Eosin staining, and images were acquired with the Aperio digital scanner microscope. Tissue sections were evaluated for tumor morphology with the use of ImageScope

software (Leica Biosystem). Adjacent sections were fixed with acetone and nonspecific immunoglobulin binding was blocked by incubating the sections with 3% BSA in PBS. Sections were then incubated with the primary antibody, a rat anti-human HER-2 (clone ICR55; ThermoFisher Scientific, Waltham, MA, USA), followed by incubation with the secondary antibody, a goat anti-rat antibody coupled to AlexaFluor555 (ThermoFisher Scientific, Waltham, MA, USA). After washing, nuclei were counterstained by incubation with DAPI (ThermoFisher Scientific, Waltham, MA, USA). Finally, sections were mounted with aqueous mounting medium (Dako, Agilent) and sealed with a coverslip. The slides were acquired with Aperio fluorescence scanner microscope (Leica Biosystem).

Western Blot

In order to verify HER-2 expression in OE-19 tumors, after excision, tumor masses were frozen in liquid nitrogen and stored at -80°C . The whole protein content was extracted by placing the samples in an adequate volume of Lysis Buffer (Tris-HCl 50 mM pH 8, NaCl 150 mM, EDTA 1 mM, NaF 100 mM, glycerol 10%, MgCl_2 1 mM, TritonX-100 1%, protease inhibitors) and subsequent disruption with Bertin Precellys homogenizer, 3 cycles at 6500 rpm, cooled. After a further 30 min incubation in a cooled rotating wheel, centrifugation at 13,200 rpm at 4°C for 15 min allowed to pellet nuclei and undisturbed material, whereas the supernatant was collected for protein analysis. The protein content of the supernatant was quantified with bicinchoninic acid (BCA) method. Proteins were separated according to their molecular weight by SDS-PAGE electrophoresis (7.5% polyacrylamide gel in non-reducing denaturing conditions) and blotted onto nitrocellulose membranes, the latter were cut before probing with the anti-HER-2 (clone ICR55; ThermoFisher Scientific, Waltham, MA, USA) and anti- β -actin primary antibodies (Cell Signaling Technology, Leiden, ND). Following incubation with the secondary antibodies goat anti-rat (Invitrogen, Waltham, MA, USA) and goat anti-rabbit (Millipore Co., Bedford, MA, USA), the detection was performed by chemiluminescence, using the ChemiDoc MP Imaging system (Bio-Rad, Hercules, CA, USA).

For the quantification of HER-2 expression in the different tumor samples, different amounts of the recombinant HER-2 extracellular domain were loaded to obtain a calibration curve. Bio-Rad Image Lab software 6.0 was used to analyze the band intensity. The band intensity value was calculated as Adjusted Volume (*i.e.*, the background-adjusted volume) and interpolated with its specific linear calibration curve.

FLIM and WB correlation analysis

Five xenograft OE-19 tumors treated with NF-800 were analyzed to investigate potential relationships between FLIM response and target concentration calculated by Western Blot. Lifetime parametric maps were created with the use of FLIMfit software, and histogram distribution of lifetimes was extrapolated pixel by pixel. The maximum FLIM signal between 0.71 and 0.72 ns was correlated with the concentration of HER-2 in tumor.

Data exploration involved the use of scatter plots and Pearson correlation coefficients as statistical tools, performed with Microsoft Excel. For each sample ($n=5$), the number of pixels that showed a lifetime between 0.70 and 0.72 ns was plotted against HER-2 quantification from WB analysis. The intuitive representations from scatter plot provide initial insights before diving into quantitative measures like Pearson correlation coefficients.

Statistical analysis

Statistical analysis was performed using Prism software (GraphPad by Dotmatics) applying test indicated in the results.

Data availability

The datasets generated and/or analysed during the current study are not publicly available due Company's confidentiality policy but are available from the corresponding author on reasonable request.

Received: 8 April 2025; Accepted: 5 December 2025

Published online: 19 December 2025

References

- van Dam, G. M. et al. Intraoperative tumor-specific fluorescence imaging in ovarian cancer by folate receptor- α targeting: first in-human results. *Nat Med.* **17**(10), 1315–1319. <https://doi.org/10.1038/nm.2472> (2011) (PMID: 21926976).
- Mieog, J. S. D. et al. Fundamentals and developments in fluorescence-guided cancer surgery. *Nature Reviews in Clinical Oncology* **19**, 9–22 (2022).
- Marston, J. C. et al. Panitumumab-IRDye800CW for Fluorescence-Guided Surgical Resection of Colorectal Cancer. *J Surg Res.* **239**, 44–51. <https://doi.org/10.1016/j.jss.2019.01.065> (2019).
- Solmaz, A. A. et al. Comparison of HER2-Targeted Antibodies for Fluorescence-Guided Surgery in Breast Cancer", *Molecular Imaging*, vol. **2021**, Article ID 5540569, 12 pages, 2021. <https://doi.org/10.1155/2021/5540569>
- Thurber, G. M., Schmidt, M. M. & Wittrup, K. D. Antibody tumor penetration: Transport opposed by systemic and antigen-mediated clearance. *Adv. Drug Delivery Rev.* **60**, 1421 (2008).
- Mortimer, J. E. et al. Functional imaging of human epidermal growth factor receptor 2-positive metastatic breast cancer using (64) Cu-DOTAtrastuzumab PET. *J. Nucl. Med.* **55**, 23–29 (2014).
- Frejd, F. & Kim, K. T. Affibody molecules as engineered protein drugs. *Exp Mol Med* **49**, e306. <https://doi.org/10.1038/emmm.2017.35> (2017).
- Ayat NR., et al. Effective MR Molecular Imaging of Triple Negative Breast Cancer With an EDB-Fibronectin-Specific Contrast Agent at Reduced Doses. *Frontiers in Oncology* **9**, (2019).
- Goux, M. et al. Nanofitin as a New Molecular-Imaging Agent for the Diagnosis of Epidermal Growth Factor Receptor Over-Expressing Tumors. *Bioconjug. Chem.* **28**(9), 2361–2371. <https://doi.org/10.1021/acs.bioconjchem.7b00374> (2017).
- Kasspooles, M., Moore, J. H., Orringer, M. B. & Beer, D. G. Amplification and over-expression of the EGFR and erbB-2 genes in huma esophageal adenocarcinomas. *Int J Cancer* **54**, 219–223 (1993).

11. Walch, A. et al. Her-2/neu gene amplification, elevated mRNA expression, and protein overexpression in the metaplasia-dysplasia-adenocarcinoma sequence of Barrett's esophagus. *Lab Invest* **81**, 791–801 (2001).
12. Dahlberg, P. S. et al. ERBB2 Amplifications in Esophageal Adenocarcinoma. *Ann Thorac Surg* **78**, 1790–1800 (2004).
13. Egebjerg K, Garbyal RS, Preuss Hasselby J, Baeksgaard L, Mau-Sørensen M, Prevalence of HER2 overexpression and amplification in squamous cell carcinoma of the esophagus: A systematic review and meta-analysis. *Critical Reviews in Oncology/Hematology*, **161**, 2021.
14. Ohashi, S. et al. Recent Advances From Basic and Clinical Studies of Esophageal Squamous Cell Carcinoma. *Gastroenterology* **149**(7), 1700–1715 (2015).
15. Rizk, N. et al. The impact of complications on outcomes after resection for esophageal and gastroesophageal junction carcinoma. *J Am Coll Surg* **198**(1), 42–50 (2016).
16. Schaafsma, B. E. et al. The clinical use of indocyanine green as a nearinfrared fluorescent contrast agent for image-guided oncologic surgery. *J Surg Oncol* **104**(3), 323–332 (2011).
17. Sun Y, et al. Fluorescence lifetime imaging microscopy for brain tumor image-guided surgery. *J Biomed Opt.* 2010 Sep-Oct; **15**(5):056022.
18. Rice, W. L., Shcherbakova, D. M., Verkhusha, V. V. & Kumar, A. T. N. In vivo tomographic imaging of deep seated cancer using fluorescence lifetime contrast. *Cancer Res* **75**, 1236–1243 (2015).
19. Pal, R., Kang, H., Choi, H. S. & Kumar, A. T. N. Fluorescence lifetime-based tumor contrast enhancement using an EGFR antibody-labeled near-infrared fluorophore. *Clin Cancer Res* **25**, 6653–6661 (2019).
20. Pal, R. et al. First Clinical Results of Fluorescence Lifetime-enhanced Tumor Imaging Using Receptor-targeted Fluorescent Probes. *Clin Cancer Res* **28**, 2373–2384 (2022).
21. Gros, S. J. et al. Effective Therapeutic Targeting of the Overexpressed HER-2 Receptor in a Highly Metastatic Orthotopic Model of Esophageal Carcinoma. *Mol Cancer Ther* **9**(7), 2037–2045 (2010).
22. Huet, S. et al. Targeted Nanofitin-drug Conjugates Achieve Efficient Tumor Delivery and Therapeutic Effect in an EGFRpos Mouse Xenograft Model. *Mol Cancer Ther.* **22**(11), 1343–1351. <https://doi.org/10.1158/1535-7163.MCT-22-0805>. PMID:37578807;PMCID:PMC10618730 (2023).
23. Bruno, R. et al. Population pharmacokinetics of trastuzumab in patients with HER2+ metastatic breast cancer. *Cancer Chemother Pharmacol.* **56**(4), 361–369 (2005).
24. Alcalá, J. R., Gratton, E. & Prendergast, F. G. Interpretation of fluorescence decays in proteins using continuous lifetime distributions. *Biophys. J.* **51**(6), 925–936 (1987).
25. Leung K. IRDye800CW-Cyclic albumin-binding domain (Ac-RLIEDICLPRWGCLWEDDK-NH2) 2011 Dec 19 [Updated 2012 Mar 1]. In: *Molecular Imaging and Contrast Agent Database (MICAD)* [Internet]. Bethesda (MD): National Center for Biotechnology Information (US); 2004–2013. Available from: <https://www.ncbi.nlm.nih.gov/books/NBK84430/>
26. Jisha, V. S., Arun, K. T., Hariharan, M. & Ramaiah, D. Site-selective binding and dual mode recognition of serum albumin by a squaraine dye. *J. Am. Chem. Soc.* **128**(18), 6024–6025 (2006).
27. Berezin, M. Y., Lee, H., Akers, W., Nikiforovich, G. & Achilefu, S. Fluorescent Lifetime of near infrared dyes for structural analysis of serum albumin. *Proc. of SPIE* **6867**, 68670J-168671 (2008).
28. Turner, D. C. & Brand, L. Quantitative Estimation of Protein Binding Site Polarity Fluorescence of A-Arylamino naphthalenesulfonates. *Biochemistry* **7**, 4A – 3780 (1968).
29. Iaboni, M. et al. Complete preclinical evaluation of the novel antibody mimetic Nanofitin-IRDye800CW for diverse non-invasive diagnostic applications in the management of HER-2 positive tumors. *Sci Rep* **15**, 9832 (2025).
30. Maadi, H., Soheilifar, M. H., Choi, W.-S., Moshtaghian, A. & Wang, Z. Trastuzumab Mechanism of Action; 20 Years of Research to Unravel a Dilemma. *Cancers* **13**, 3540 (2021).
31. Ranaudo, A. et al. Guiding Competitive Binding Assays Using Protein-Protein Interaction Prediction: The HER2-Affitin Use Case. *ACS Omega* **9**(50), 49522–49529 (2024).
32. Ullén, A. et al. Prostate cancer cell lines lack amplification: Overexpression of HER2. *Acta Oncol.* **44**(5), 490–495. <https://doi.org/10.1080/02841860510029888> (2005).
33. Sanjay Pant, H.B. Tripathi, D.D. Pant, Solvent polarity and viscosity effect on the fluorescence spectrum and excited state lifetime of quinine dication, *Journal of Photochemistry and Photobiology A: Chemistry*, **(85)**1–2: 33–38 (1995).
34. Ávila-Moreno, F. Nanofitins and their applications in human health and lung diseases. *Mol. Ther.* **31**(10), 2813–2814 (2023).
35. Pal, R. et al. Fluorescence lifetime of injected indocyanine green as a universal marker of solid tumours in patients. *Nat. Biomed. Eng* **7**, 1649–1666 (2023).
36. Liu, C., Zhao, T., He, S., Zhao, L. & Zeng, X. *J. Mater. Chem. B* <https://doi.org/10.1039/D0TB01329C> (2020).
37. Butte PV, Mamelak AN, Nuno M, Bannykh SI, Black KL, Marcu L. Fluorescence lifetime spectroscopy for guided therapy of brain tumors. *Neuroimage.* 2011 Jan; **54** Suppl 1(Suppl 1):S125–35. <https://doi.org/10.1016/j.neuroimage.2010.11.001>. Epub 2010 Nov 3. PMID: 21055475; PMCID: PMC3335732.
38. Yankelevich, D. R. et al. Design and evaluation of a device for fast multispectral time-resolved fluorescence spectroscopy and imaging. *Rev Sci Instrum.* **85**(3), 034303. <https://doi.org/10.1063/1.4869037>. PMID:24689603;PMCID:PMC3971822 (2014).
39. Boppart, S. A. et al. Label-free optical imaging technologies for rapid translation and use during intraoperative surgical and tumor margin assessment. *J Biomed Opt.* **23**(2), 1–10. <https://doi.org/10.1117/1.JBO.23.2.021104>. PMID:29288572;PMCID:PMC5747261 (2017).
40. Gouzou, D. et al. *Methods Appl. Fluoresc.* **12**, 022001 (2024).
41. Lin, Y. et al. Coupling a recurrent neural network to SPAD TCSPC systems for real-time fluorescence lifetime imaging. *Sci Rep* **14**, 3286 (2024).

Acknowledgements

The authors would like to thank Gabriella Monaco, MD for her remarkable support during animal studies; Claudia Cabella, PhD for her invaluable guidance and support throughout this project and Fluody for the collaboration in the project Flimag.

Author contributions

F.L.C., F.A., F.B., A.M., L.P. and E.R. designed research; F.L.C., F.A., D.F., M.I., F.C., A.C., M.R., F.P., F.S and E.R. performed research; F.F., and G.V. built the inhouse microscope and wrote the software; F.L.C., F.A., D.F., M.I., F.C., A.C., M.R. and F.P. analyzed data; and F.L.C., F.A., M.I., F.F., M.C., S.H., L.P. and E.R. wrote the paper. All authors reviewed the manuscript. Francesca La Cava and Francesca Arena contributed equally.

Funding

Regione Piemonte, Italy POR FESR 2014/2020 –PRISM-E.

Declarations

Competing interests

The authors declare no competing interests.

Additional information

Supplementary Information The online version contains supplementary material available at <https://doi.org/10.1038/s41598-025-31872-8>.

Correspondence and requests for materials should be addressed to F.C.

Reprints and permissions information is available at www.nature.com/reprints.

Publisher's note Springer Nature remains neutral with regard to jurisdictional claims in published maps and institutional affiliations.

Open Access This article is licensed under a Creative Commons Attribution-NonCommercial-NoDerivatives 4.0 International License, which permits any non-commercial use, sharing, distribution and reproduction in any medium or format, as long as you give appropriate credit to the original author(s) and the source, provide a link to the Creative Commons licence, and indicate if you modified the licensed material. You do not have permission under this licence to share adapted material derived from this article or parts of it. The images or other third party material in this article are included in the article's Creative Commons licence, unless indicated otherwise in a credit line to the material. If material is not included in the article's Creative Commons licence and your intended use is not permitted by statutory regulation or exceeds the permitted use, you will need to obtain permission directly from the copyright holder. To view a copy of this licence, visit <http://creativecommons.org/licenses/by-nc-nd/4.0/>.

© The Author(s) 2025